

INTERIOR EIGENSOLVER BASED ON RATIONAL FILTER WITH COMPOSITE RULE

YUER CHEN* AND YINGZHOU LI†

Abstract. Contour integral based rational filter leads to interior eigensolvers for non-Hermitian generalized eigenvalue problems. Based on the Zolotarev's problems, this paper proves the asymptotic optimality of the trapezoidal quadrature of the contour integral in terms of the rational function separation. A composite rule of the trapezoidal quadrature is derived. Two interior eigensolvers are proposed based on the composite rule. Both eigensolvers adopt direct factorization and multi-shift generalized minimal residual method for the inner and outer rational functions, respectively. The first eigensolver fixes the order of the outer rational function and applies the subspace iteration to achieve convergence, whereas the second eigensolver doubles the order of the outer rational function every iteration to achieve convergence without subspace iteration. The efficiency and stability of proposed eigensolvers are demonstrated on synthetic and practical sparse matrix pencils.

Key words. Generalized eigenvalue problem; non-Hermitian matrix; contour integral; trapezoidal quadrature; optimal rational approximation; Zolotarev problem.

1. Introduction. We aim to solve the large-scale interior eigenvalue problem for non-Hermitian matrices. Such problems arise from many fields including but not limited to electronic structure calculations, dynamic system simulations, control theory, etc. Most of these applications only require part of eigenvalues of interest, and many of which are interior eigenvalues.

The interior non-Hermitian generalized eigenvalue problem we consider is

$$(1.1) \quad Ax_i = \lambda_i Bx_i, \quad \lambda_i \in \mathcal{D},$$

where \mathcal{D} is the region of interest, matrix pencil (A, B) is regular, and either or both of A and B is non-Hermitian. The goal is to find all eigenpairs (λ_i, x_i) in the region \mathcal{D} . Once the problem in a \mathcal{D} region can be solved, the entire spectrum could be partitioned into a union of many regions. The interior eigensolver could be applied to all regions in parallel to obtain the full eigendecomposition.

Methods for non-Hermitian generalized eigenvalue problems have been developed for decades. The QZ method [9] is a popular one in practice for dense and small-to-medium scale matrices. When a sparse and large-scale matrix is considered, iterative methods [7, 17] are preferred. Among iterative methods, many adopt the combination of a contour-based filter and the subspace iteration, e.g., Sakurai-Sugiura (SS) method [15] and variants of FEAST method [13, 8]. The original SS method suffers from numerical instability due to the ill-conditioned Hankel matrix. Then Sakurai and Sugiura proposes CIRP [4], which uses Rayleigh-Ritz projection to avoid the explicit usage of the momentum and block version SS method [5]. The number of linear systems therein is reduced, and so is the order of the Hankel matrix. The FEAST method originally proposed for Hermitian matrices is extended to non-Hermitian matrices and results in many variants, dual FEAST [6], BFEAST [19], HFEAST [18], etc. For all the contour-based filters or rational filters in the methods above, the convergence and convergence rate highly depend on the locations and weights of poles. Although the trapezoidal quadrature leads to a good convergence behavior [6], its optimality remains unknown for non-Hermitian matrices. In this paper, we discuss the optimality of the trapezoidal quadrature and its composite rule property. On the

*School of Mathematical Sciences, Fudan University, Shanghai, China.

†School of Mathematical Sciences, Fudan University, Shanghai, China (yingzhouli@fudan.edu.cn).

top of the property, we propose interior eigensolvers for non-Hermitian generalized eigenvalue problems.

Our contributions in this paper can be summarized in two parts: theoretical analysis and algorithm design. Theoretically, with the tool of Zolotarev's problems, we prove that when the contour is a circle, the inverse power method leads to an optimal rational separation for a non-Hermitian generalized eigenvalue problem. The trapezoidal quadrature of a contour integral achieves asymptotically optimality in separation. A composite formula for the trapezoidal quadrature is proposed to facilitate the later algorithm design. More specially, given a rational function $R_k(z)$ from the trapezoidal quadrature, we derive the composite formula as $R_k(z) = R_{k_2}(T(R_{k_1}(z)))$ for $k = k_1 k_2$ and $T(\cdot)$ being a Möbius transform. In the algorithm design part, we propose two novel algorithms based on the composite formula of the trapezoidal quadrature. The first algorithm adopts k_1 and k_2 as hyperparameters and applies the subspace iteration with the fixed filter $R_{k_2}(T(R_{k_1}(z)))$ to matrix pencils. The inner rational function R_{k_1} is implemented with direct matrix factorization, whereas the outer rational function R_{k_2} is implemented via the multi-shift generalized minimal residual method (GMRES). The second algorithm adopts k_1 as a hyperparameter and removes the subspace iteration. The convergence of the second algorithm is guaranteed by doubling k_2 every iteration until the rational approximation is accurate enough. Similar to the first algorithm, the inner and outer rational functions are implemented via direct factorization and multi-shift GMRES, respectively. Thanks to the nature of multi-shift GMRES, doubling k_2 does not significantly increase the computational cost. Numerical results on both synthetic and practical matrix pencils demonstrate the efficiency of the two proposed algorithms. Both theoretically and numerically, the second algorithm is suggested for practical usage.

The rest of this paper is organized as follows. In [section 2](#), we introduce the basic idea and practical consideration of the contour integral based filter. Later, we introduce the Zolotarev third and fourth problems with related theorems and the optimalities of rational function separation in [section 3](#). Two algorithms are proposed in [section 4](#). Then, numerical experiments demonstrate the efficiency of both proposed algorithms in [section 5](#). Finally, [section 6](#) concludes the paper.

2. Subspace iteration with rational filter. Subspace iteration with rational filter is a class of eigensolvers for interior non-Hermitian generalized eigenvalue problems [\(1.1\)](#). All eigensolvers in this class use the subspace iteration framework and adopt various filters, i.e., rational functions with different choices of weights and poles. These rational filters include various discretizations of the contour enclosing \mathcal{D} , which is the desired region of eigenvalues. In this section, we will first review the subspace iteration and then discuss contour-based rational filters with various discretization strategies. Some practical considerations, i.e., the number of vectors and the number of poles, are discussed in the end.

2.1. Subspace iteration. The general framework of the subspace iteration with filter iterates between two phases: 1) refining the subspace via filter; 2) solving a reduced eigenvalue problem in the subspace.

In the first phase, the filter is applied to an approximated basis of the subspace, and a refined representation of the subspace is obtained. For Hermitian eigenvalue problems, left and right eigen-subspaces are identical. Hence, only the basis of the right eigen-subspace is usually refined, and its complex conjugate is used as that of the left eigen-subspace. However, for non-Hermitian eigenvalue problems, left and right eigen-subspaces are different. After the right eigen-subspace is refined, an extra

step is needed to obtain an approximation of the left eigen-subspace. In the second phase, the original large-scale eigenvalue problem is projected to the left and right eigen-subspaces and reduced to an eigenvalue problem of a much smaller scale. Then the small-scale eigenvalue problem is solved by classical dense eigensolvers, which results in the approximated eigenvalues of the original problem. The approximated eigenvectors could be calculated as well. Some filters depend on the approximated eigenvalues, whereas others do not. For filters that do not use the approximated eigenvalues, the second phase serves as a calculation of the stopping criteria.

Due to the potential ill-conditioned eigenbasis of non-Hermitian matrices, the generalized Schur vectors could be extracted to represent the eigen-subspaces and lead to a more stable scheme. Such a subspace iteration idea has been combined with FEAST for non-Hermitian matrices and results in HFEAST [18]. Let U be the vectors approximating the right eigen-subspace, i.e., U is the result of applying the filter. The orthonormal basis of U is denoted as $V = \text{orth}(U)$. As in HFEAST [18], the orthonormal basis of the left eigen-subspace could be constructed as $W = \text{orth}(AV - \sigma BV)$, where σ is the shift different from the eigenvalues of (A, B) . After obtaining the approximated orthonormal bases of the left and right eigen-subspace, the reduced generalized eigenvalue problem (W^*AV, W^*BV) is addressed by the QZ algorithm and yields the generalized Schur form,

$$P_L^*(W^*AV)P_R = H_A \quad \text{and} \quad P_L^*(W^*BV)P_R = H_B,$$

where P_L and P_R are orthogonal matrices, H_A and H_B are upper triangular matrices. The approximated eigenvalues are,

$$\tilde{\lambda}_i = (H_A)_{i,i} / (H_B)_{i,i},$$

for $i = 1, 2, \dots, s$. To obtain the eigenvectors, we further calculate the left and right eigenvectors of (H_A, H_B) and denote them as V_L and V_R respectively. The approximated left and right eigenvectors of (A, B) are, respectively,

$$WP_LV_L \quad \text{and} \quad VP_RV_R.$$

Algorithm 2.1 Subspace Iteration with Filter

Input: matrix pencil (A, B) , region \mathcal{D} , number of eigenvalues s , shift σ .

Output: All eigenpairs (λ_i, x_i) , $\lambda_i \in \mathcal{D}$.

- 1: Generate random $Y^{N \times n_{\text{col}}}$, $n_{\text{col}} \geq s$
 - 2: **while** not converge **do**
 - 3: $U = \rho(B^{-1}A)Y$
 - 4: $V = \text{orth}(U)$
 - 5: $W = \text{orth}(AV - \sigma BV)$
 - 6: $[H_A, H_B, P_L, P_R, V_L, V_R] = \text{qz}(W^*AV, W^*BV)$
 - 7: $\tilde{\lambda}_i = (H_A)_{i,i} / (H_B)_{i,i}$
 - 8: $Y = VP_RV_R$
 - 9: **end while**
-

The overall framework of the subspace iteration in HFEAST [18] with filter $\rho(\cdot)$ is summarized in Algorithm 2.1. In the rest paper, we adopt the subspace iteration as in Algorithm 2.1 and focus on the construction of $\rho(\cdot)$.

2.2. Contour based filter and discretization. The basic idea behind the filter is to construct a matrix function whose value is close to zero outside the region \mathcal{D} and different from zero inside \mathcal{D} . One good choice of matrix functions is the indicator function of \mathcal{D} , which could be constructed via a contour integral enclosing the region \mathcal{D} . The indicator function of \mathcal{D} via contour integral admits,

$$(2.1) \quad f(z) = \frac{1}{2\pi i} \oint_{\Gamma} \frac{1}{\zeta - z} d\zeta = \begin{cases} 1, & z \in \mathcal{D} \\ 0, & z \notin \mathcal{D} \end{cases},$$

where Γ is the positively oriented Jordan curve boundary encloses the region \mathcal{D} .¹

For a diagonalizable matrix pencil (A, B) , i.e.,

$$AX = BXA,$$

with X being the eigenvectors and Λ is a diagonal matrix with eigenvalues on its diagonal, the indicator function $f(z)$ applying to matrices becomes

$$(2.2) \quad \begin{aligned} f(B^{-1}A) &= \frac{1}{2\pi i} \oint_{\Gamma} (\zeta I - B^{-1}A)^{-1} d\zeta \\ &= X \left[\frac{1}{2\pi i} \oint_{\Gamma} (\zeta I - \Lambda)^{-1} d\zeta \right] X^{-1} = X \mathbb{1}_{\mathcal{D}}(\Lambda) X^{-1}, \end{aligned}$$

where $\mathbb{1}_{\mathcal{D}}(\cdot)$ denotes the indicator function for region \mathcal{D} . In [19], a result similar to (2.2) is proved, which contributes to the theoretical foundation that the contour integral works even if the non-Hermitian system is defective.

Various numerical discretizations of the contour integral (2.2) lead to the various filters. In many applications, especially non-Hermitian eigenvalue problems, the contour Γ is circular. In many other applications, the contour could be conformally mapped to a circle. Hence, in this paper, we will discuss the discretization of contour integrals for Γ being a circle. When the contour is a unit circle, we could reparameterize the circle by $e^{i\theta}$ for $\theta \in [0, 2\pi)$. The integral (2.1), then, is a one-dimensional integral and could be numerically evaluated by various quadrature rules. Generally, the discretized integral with k points could be written as

$$(2.3) \quad R_k(z) = \sum_{i=1}^k \frac{w_i}{p_i - z},$$

where $\{w_i\}_{i=1}^k$ are weights, $\{p_i\}_{i=1}^k$ are poles. For example, when the trapezoidal quadrature is applied, the integral (2.1) is numerically approximated by

$$R_k^{(T)}(z) = \frac{1}{k} \sum_{i=1}^k \frac{e^{i\theta_i}}{e^{i\theta_i} - z},$$

where $\theta_i = \frac{2(i-\frac{1}{2})\pi}{k}$. From the form of (2.3), we notice that $R_k(z)$ is a rational function. Let $\mathcal{R}_{n,m} = \{P(z)/Q(z) : \deg(P(z)) \leq n, \deg(Q(z)) \leq m\}$ be the set of rational functions, where $P(z)$ and $Q(z)$ are polynomials and $\deg(\cdot)$ denotes the degree of the polynomial. The discretized contour integral (2.3) is in $\mathcal{R}_{k-1,k}$.

¹In (2.1), we implicitly assume that the eigenvalues of (A, B) do not locate on the boundary of \mathcal{D} .

When the discretized contour integral applies to matrices, the rational matrix function yields

$$(2.4) \quad R_k(B^{-1}A) = \sum_{i=1}^k w_i(p_i I - B^{-1}A)^{-1} = \sum_{i=1}^k w_i(p_i B - A)^{-1} B.$$

The matrix function $R_k(B^{-1}A)$ in (2.4) is used as the filter in Algorithm 2.1.

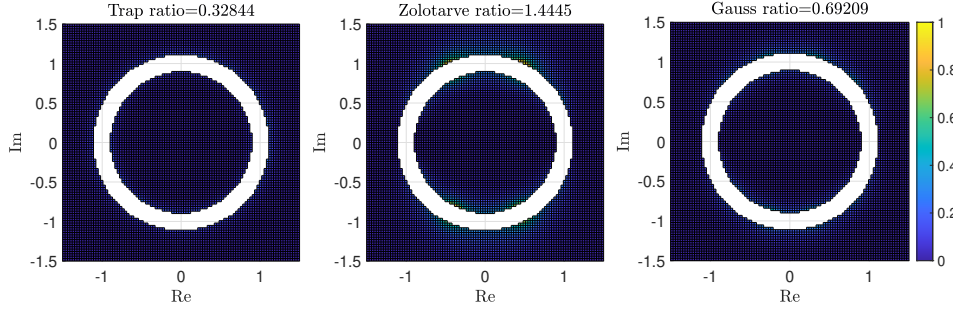


FIG. 2.1. Approximation errors to the step function on the complex plane except an annulus $\{x : 1/1.1 < |x| < 1.1\}$ for trapezoidal quadrature (left), Zolotarev's function (middle) and Gauss quadrature (right). Here 16 poles are adopted for all three rules. The figure shows the approximation error to indicator function on complex plane.

Among various quadrature rules, the optimal quadrature needs to be decided based on a criterion. As we will see later, the convergence rate of subspace iteration mainly depends on the ratio (2.7). Since we do not know eigenvalues in a priori, we could assume that there is an annulus around the boundary of \mathcal{D} as a generalized eigengap. The inner part and the outer part are,

$$I = \{z : |z| \leq a\}, \quad \text{and} \quad O = \{z : |z| \geq b\},$$

where a and b are the radii of the inner and outer parts of the annulus, I contains all the eigenvalues inside \mathcal{D} . Then the criterion is defined as,

$$(2.5) \quad \mathfrak{R} = \frac{\sup_{z \in O} |R_k(z)|}{\inf_{z \in I} |R_k(z)|}.$$

When the ratio is small, the convergence of the subspace iteration is fast. Hence, we would like to address the following optimization problem to obtain the optimal weights and poles for a given k ,

$$(2.6) \quad \inf_{\{w_i\}_{i=1}^k, \{p_i\}_{i=1}^k} \frac{\sup_{z \in O} |R_k(z)|}{\inf_{z \in I} |R_k(z)|}.$$

From (2.6), what we want is to separate the values inside and outside by enlarging the values in I and reducing the values in O at the same time. Following the above argument, the contour is not necessarily the boundary of \mathcal{D} and we can choose any contour in the annulus,

$$\text{annu}(a, b) = \{z : a \leq |z| \leq b\}.$$

Moreover, we could discard the concept of contour discretization and view it as a rational function separation problem. One could imagine that as $b - a$ becomes larger,

it is easier to separate the values inside and outside the annulus with rational functions. The drawback of using a larger b is that more eigenvalues may fall into $\text{annu}(a, b)$ and we do not explicitly know the impact of these eigenvalues on the convergence of the subspace iteration.

Figure 2.1 illustrates the approximation error to the step function and the criteria ratio \mathfrak{R} for three numerical discretizations of $R_k(z)$ with 16 poles, namely the trapezoidal quadrature, Zolotarev fourth function [8] on real axis, and the Gauss quadrature. As shown in Figure 2.1, the Zolotarev fourth function on real axis is neither optimal for non-Hermitian eigenvalue problems in the L^∞ sense nor optimal in (2.6) sense when the inner and outer part no longer defined on real axis. The trapezoidal quadrature outperforms the other two. As one of the contributions in this paper, we prove in Theorem 3.5 that trapezoidal quadrature provides the asymptotically optimal weights and poles for (2.6).

2.3. Practical consideration. Given a discretization rule, the major computational cost in applying the filter $R_k(B^{-1}A)Y$ as in (2.4) lies in solving the shifted linear systems, $(p_i B - A)^{-1}$ for $i = 1, \dots, k$. Such a computational cost is often determined by the condition number of $(p_i B - A)$. Since the positions of poles are on the contour, the condition number is inversely proportional to the eigengap around the contour, which is in general large in practice. Hence, in most contour based filters, the shifted linear systems are solved by direct methods, e.g., LU factorization. The overall computational cost is then divided into two parts: the offline factorization part and the online solving part (backward substitution). The cost could be rewritten as

$$C_{\text{factor}} \times k + C_{\text{apply}} \times k \times n_{\text{col}} \times n_{\text{iter}} + o(C_{\text{apply}}),$$

where C_{factor} is the cost of a factorization, C_{apply} is the cost of a backward substitution, k is the number of poles, n_{col} is the number of columns in Y , n_{iter} is the number of subspace iterations, and $o(C_{\text{apply}}) = o(C_{\text{apply}}(N))$ is the rest cost of a lower order than $C_{\text{apply}}(N)$. Throughout the subspace iterations, the tuneable hyperparameters are k and n_{col} , and n_{iter} is determined by k , n_{col} , and the stopping criteria in the algorithm. The dependence of n_{iter} on k and n_{col} could be reflected by the function value gap of $R_k(\lambda_i)$, since we are essentially applying power method with $R_k(B^{-1}A)$. Let σ be a permutation of $1, 2, \dots, N$, such that

$$|R_k(\lambda_{\sigma_1})| \geq |R_k(\lambda_{\sigma_2})| \geq \dots \geq |R_k(\lambda_{\sigma_N})|.$$

Then, the number of subspace iteration n_{iter} mainly depends on the ratio,

$$(2.7) \quad \max_{i > n_{\text{col}}} |R_k(\lambda_{\sigma_i})| \bigg/ \min_{\lambda_{\sigma_i} \in \mathcal{D}} |R_k(\lambda_{\sigma_i})|.$$

When the ratio is greater or equal to one, then the subspace iteration would suffer from a divergence issue. When the ratio is smaller than one, the subspace iteration would converge and the convergence rate depends on the distance between the ratio and one. The further the distance, the faster the convergence. In the following, we discuss the practical consideration for the number of vectors n_{col} and the number of poles k .

Number of vectors n_{col} . To extract the entire eigenspace we are interested, it is necessary that $n_{\text{col}} \geq s$. However, the number of eigenvalues in the region \mathcal{D} is not known a priori. Usually, a rough estimation of s , denoted as \tilde{s} , is calculated and the number of vectors is set as $n_{\text{col}} = \lfloor \rho \tilde{s} \rfloor$ for ρ being a hyperparameter greater than

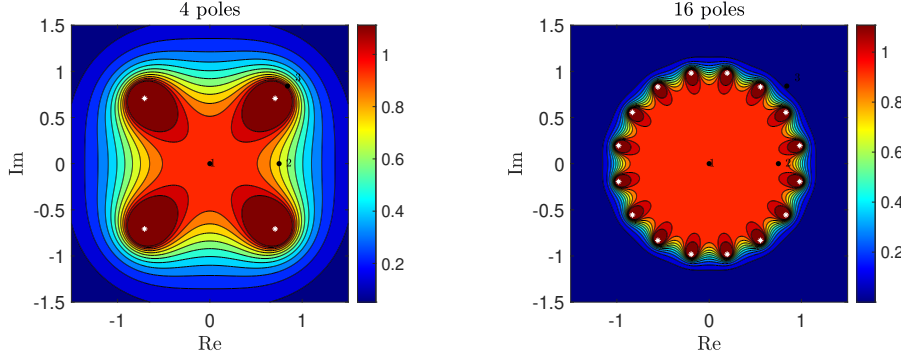


FIG. 2.2. Filled contour plots for trapezoidal quadrature of the contour integral with 4 poles (Left) and 16 poles (Right). The matrix pair has two desired eigenpairs with eigenvalues being $\lambda_1 = 0$ and $\lambda_2 = 0.75$, and an unwanted eigenpair with eigenvalue being $\lambda_3 = \sqrt[4]{2}e^{i\pi/4}$. In the left figure, the function values are $|R_4^{(T)}(\lambda_1)| = 1$, $|R_4^{(T)}(\lambda_2)| \approx 0.7596$, and $|R_4^{(T)}(\lambda_3)| = 1$. In the right figure, the function values are $|R_{16}^{(T)}(\lambda_1)| = 1$, $|R_{16}^{(T)}(\lambda_2)| \approx 0.9901$, and $|R_{16}^{(T)}(\lambda_3)| = 0.0667$. The white stars indicate the locations of the poles.

one. Since the estimation of s is not in the scope of this paper, we set $n_{\text{col}} = \lfloor \rho s \rfloor$ in all numerical experiments. Even when we have $n_{\text{col}} \geq s$, the subspace iteration may still fail to converge to all the desired eigenpairs. We provide an example of such cases in Figure 2.2. There are 2 eigenvalues $\lambda_1 = 0$ and $\lambda_2 = 0.75$ inside \mathcal{D} , and an eigenvalue $\lambda_3 = \sqrt[4]{2}e^{i\pi/4}$ outside. As in the Figure 2.2 Left, when 4 poles are adopted, the function values obey $1 = |R_4^{(T)}(\lambda_3)| > |R_4^{(T)}(\lambda_2)| \approx 0.7596$. The ratio (2.7) is greater than one, and the iteration with two columns would converge to (λ_1, x_1) and (λ_3, x_3) other than desired eigenpairs. The overall subspace iteration fails to capture all the desired eigenpairs inside \mathcal{D} . One way to deal with the issue is to increase n_{col} until it covers all eigenvalues whose function values are greater than $R_4^{(T)}(\lambda_2)$ and make the ratio (2.7) smaller than one. Even when convergence is guaranteed, we may still increase n_{col} for faster convergence. However, when there are many unwanted eigenvalues close to the contour, we need to set n_{col} extremely large for the subspace iteration to converge. In this case, it would be more efficient to increase the number of poles.

Number of poles k . In many applications, for stable convergence, adding poles is an inevitable choice. When more poles are added, i.e., $f(z)$ has been discretized with more points, the numerical approximation of $R_k(z)$ to $f(z)$ is improved. The ratio (2.7) is guaranteed to be smaller than one even when $n_{\text{col}} = s$. For example, as in Figure 2.2 Right, the number of poles is increased from 4 to 16. Then we have function values $|R_{16}^{(T)}(\lambda_1)| = 1$, $|R_{16}^{(T)}(\lambda_2)| \approx 0.9901$, and $|R_{16}^{(T)}(\lambda_3)| \approx 0.0667$, and the ratio (2.7) becomes $|R_{16}^{(T)}(\lambda_3)|/|R_{16}^{(T)}(\lambda_2)| \approx 0.0594$ away from one. The subspace iteration would converge efficiently even when $n_{\text{col}} = 2$. Adding the number of poles leads to a more accurate approximation to $f(z)$, and, hence, a smaller n_{col} and n_{iter} . The drawback of increasing the number of poles is the increasing number of matrix factorizations, which is computationally more expensive than that of solving (the backward substitution). When a massive amount of computational resources are available, all k poles could be calculated independently and in parallel. Hence, in practice, we would increase k to benefit most from computational resources and then

increase n_{col} to have an efficient and robust subspace iteration algorithm.

3. Asymptotically optimal contour discretization. This section shows that the trapezoidal quadrature is an asymptotically optimal discretization for a disk region \mathcal{D} , i.e., an asymptotically optimal solution to the min-max problem (2.6). In subsection 3.1, Zolotarev third and fourth problems are reviewed. The former serves as the theoretical foundation of the asymptotic optimality of trapezoidal quadrature. Then subsection 3.2 derives that $R_k^{(T)}(z) = R_1^{(T)}(z^k)$, which serves as a compact form for $R_k^{(T)}(z)$. For the sake of notations, we abuse $R_k(z) = R_k^{(T)}(z)$ in the rest paper, which represents the trapezoidal quadrature of the unit circle contour whose center is located at the origin. When the radii of the contour is r and the center is c , we denote the discretization as $R_{c,r,k}(z)$. Finally, we prove that the trapezoidal quadrature is an asymptotically optimal contour discretization for a disk region \mathcal{D} in subsection 3.3.

3.1. Zolotarev problems. We introduce the Zolotarev third and fourth problems with their related theoretical results [12, 16]. Zolotarev third problem proposes optimal rational functions for the separation of two regions, whereas Zolotarev fourth problem proposes the optimal uniform approximation to the sign function on two symmetric intervals. Since contour discretization admits the form of a rational function, it is natural to bridge the contour discretization and Zolotarev problems.

The Zolotarev third and fourth problems are given in Definition 3.1 and Definition 3.2, respectively.

DEFINITION 3.1. *Let E and G be two disjoint regions of \mathbb{C} , i.e., $E \cap G = \emptyset$. The Zolotarev third problem is*

$$(3.1) \quad Z_k(E, G) = \inf_{r \in \mathcal{R}_{k,k}} \frac{\sup_{z \in E} |r(z)|}{\inf_{z \in G} |r(z)|}.$$

DEFINITION 3.2. *Let $0 < \ell < 1$. The Zolotarev fourth problem is*

$$\inf_{r \in \mathcal{R}_{k,k}} \|\text{sign}(x) - r(x)\|_{L^\infty([-1, -\ell] \cup [\ell, 1])}.$$

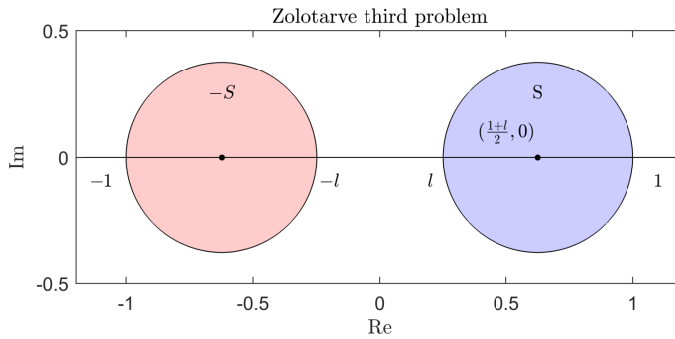


FIG. 3.1. Regions in Zolotarev third problem when E and G are symmetric disks.

The Zolotarev third problem tends to find a rational function that separates E and G most. The Zolotarev fourth problem is a special case of the third problem with the region $E = [-1, -\ell]$ and $G = [\ell, 1]$. It can be shown that the Zolotarev third problem and Zolotarev fourth problem are equivalent via a Möbius transform [12]. The

explicit solution to Zolotarev fourth problem is adopted in [8] to construct an interior eigensolver for Hermitian eigenvalue problems. More results about the Zolotarev fourth problem can be found in [12]. When E and G are symmetric disks as in Figure 3.1, the solution to Zolotarev third problem is explicitly given in Theorem 3.3. Theorem 3.3 claimed in this paper takes a different parameterized form of that in [16].

THEOREM 3.3. *Let $S = \{z \in \mathbb{C} : |z - \frac{1+\ell}{2}| \leq \frac{1-\ell}{2}\}, 0 < \ell < 1$. Then the rational function*

$$r_k^{(Z)}(z) = \left(\frac{z - \sqrt{\ell}}{z + \sqrt{\ell}} \right)^k,$$

attains the infimum of the Zolotarev third problem $Z_k(S, -S)$ and the infimum equals to $(\frac{1+\sqrt{\ell}}{1-\sqrt{\ell}})^{-2k}$.

The explicit solution to Zolotarev third problem as in Theorem 3.3 is the key to prove the asymptotical optimality of the trapezoidal quadrature for contour integral. The rational function in Theorem 3.3 is referred as the Zolotarev function in the rest paper.

3.2. Compact form for $R_k(z)$. In order to connect the Zolotarev function and the trapezoidal quadrature of the contour integral, and derive the composite formula in section 4, we establish an equality relation between $R_{k^m}(z)$ and $R_k(z^m)$. The relation heavily relies on the symmetry of trapezoidal quadrature on the circle.

Let us start with toy cases $k = 2, 4$. The trapezoidal quadrature of unit circular contour with two poles, R_2 , could be rewritten as

$$R_2(z) = \frac{1}{2} \left(\frac{e^{\frac{i\pi}{2}}}{e^{\frac{i\pi}{2}} - z} + \frac{e^{\frac{3i\pi}{2}}}{e^{\frac{3i\pi}{2}} - z} \right) = \frac{1}{2} \frac{2e^{i\pi}}{e^{i\pi} - z^2} = \frac{1}{1 + z^2} = R_1(z^2).$$

Here we use the symmetry of poles and weights with respect to the origin to derive the compact form of $R_2(z)$ and find that $R_2(z)$ is equivalent to $R_1(z^2)$. Let us further derive the compact form of $R_4(z)$,

$$\begin{aligned} R_4(z) &= \frac{1}{4} \left(\frac{e^{\frac{i\pi}{4}}}{e^{\frac{i\pi}{4}} - z} + \frac{e^{\frac{7i\pi}{4}}}{e^{\frac{7i\pi}{4}} - z} + \frac{e^{\frac{3i\pi}{4}}}{e^{\frac{3i\pi}{4}} - z} + \frac{e^{\frac{5i\pi}{4}}}{e^{\frac{5i\pi}{4}} - z} \right) \\ &= \frac{1}{2} \left(\frac{e^{\frac{i\pi}{2}}}{e^{\frac{i\pi}{2}} - z^2} + \frac{e^{\frac{3i\pi}{2}}}{e^{\frac{3i\pi}{2}} - z^2} \right) = R_2(z^2) = R_1(z^4), \end{aligned}$$

where, in the second equality, we combine the first two and last two terms, and in the last equality, we adopt the compact form of $R_2(z)$. From the derivation of the compact forms of $R_2(z)$ and $R_4(z)$, we could directly extend the derivation to obtain the compact form of $R_k(z) = R_1(z^k)$ for $k = 2^m, m \in \mathbb{N}_+$. Fortunately, the compact form holds for any $k \in \mathbb{N}_+$. The result is summarized in Lemma 3.4.

LEMMA 3.4. *For all $k \in \mathbb{N}_+$, let k roots of $z^k = -1$ be $\sigma_i^{(k)}$ for $i = 1, \dots, k$. Then the compact form of $R_k(z)$ admits,*

$$(3.2) \quad R_k(z) = \frac{1}{k} \sum_{i=1}^k \frac{\sigma_i^{(k)}}{\sigma_i^{(k)} - z} = \frac{1}{1 + z^k} = R_1(z^k).$$

Proof. We first prove two equalities, (3.3) and (3.4), and then derive the compact form of $R_k(z)$.

The k roots of the k -th degree polyWnomial $z^k + 1$ are abused as σ_i for $i = 1, 2, \dots, k$. A k -th order polynomial with k roots takes form, $a_k \prod_{i=1}^k (z - \sigma_i)$, where a_k is the coefficient in the leading order. Comparing with the leading order coefficient in $z^k + 1$, we know $a_k = 1$ and have,

$$(3.3) \quad z^k + 1 = \prod_{i=1}^k (z - \sigma_i).$$

Then we prove the second equality,

$$(3.4) \quad -\frac{1}{k} \sum_{i=1}^k \sigma_i \prod_{j=1, j \neq i}^k (z - \sigma_j) = 1.$$

The left-hand side of (3.4) is a $(k-1)$ -th degree polynomial. For the equality (3.4) to hold, we only need to check the equality on k different points. Specially, we check that on σ_i for $i = 1, \dots, k$ and obtain,

$$-\frac{\sigma_i}{k} \prod_{j=1, j \neq i}^k (\sigma_i - \sigma_j) = -\frac{\sigma_i}{k} \lim_{z \rightarrow \sigma_i} \frac{z^k + 1}{z - \sigma_i} = -\frac{\sigma_i}{k} \frac{k\sigma_i^{k-1}}{1} = -\sigma_i^k = 1,$$

where the first equality is due to (3.3) and the continuity of $(z^k + 1)/(z - \sigma_i)$, the second equality comes from the L'Hopital rule of complex functions, and the last equality holds since σ_i is a root of $z^k + 1$.

Finally, we derive the compact form of $R_k(z)$ as in Lemma 3.4.

$$\begin{aligned} R_k(z) &= \frac{1}{k} \sum_{i=1}^k \frac{\sigma_i}{\sigma_i - z} = \frac{-\frac{1}{k} \sum_{i=1}^k \sigma_i \prod_{j=1, j \neq i}^k (z - \sigma_j)}{\prod_{i=1}^k (z - \sigma_i)} \\ &= \frac{1}{\prod_{i=1}^k (z - \sigma_i)} = \frac{1}{z^k + 1} = R_1(z^k), \end{aligned}$$

where the second equality adopts (3.4) and the fourth equality adopts (3.3). \square

A related compact form without detailed derivation could be found in [5]. The compact form Lemma 3.4 could be further generalized to $R_{c,r,k}(z)$ and results the compact form,

$$R_{c,r,k}(z) = \frac{1}{1 + \left(\frac{z-c}{r}\right)^k}.$$

3.3. Optimal solution and the asymptotic optimality of trapezoidal quadrature. In this section, we prove that, if we know the desired spectrum explicitly, the rational function behind the inverse iteration achieves the optimal of (3.1) for $E = O$ and $G = I$. On the other hand, the rational function $R_k(z)$ from the trapezoidal quadrature discretization of the contour integral achieves asymptotic optimality of (3.1), i.e., the ratio \mathfrak{R} for $R_k(z)$ decays in the same rate as that of the optimal rational function up to a constant prefactor 2.

THEOREM 3.5. *The rational function*

$$(3.5) \quad \left(\frac{1}{z}\right)^k$$

achieves the infimum of the min-max problem (3.1) for $E = O$ and $G = I$. And the infimum equals to $\left(\frac{a}{b}\right)^k$.

Proof. We address Zolotarev third problem with region I and O , i.e., $Z_k(O, I)$. Define a Möbius transform $T(z) = \gamma \frac{z-\alpha}{z-\beta}$ such that

$$T(-b) = 1, \quad T(-a) = -1, \quad T(a) = -\ell, \quad T(b) = \ell.$$

The parameters γ , α , β , and ℓ are determined by a and b . They satisfy

$$\alpha = \sqrt{ab}, \quad \beta = -\sqrt{ab}, \quad \gamma = \frac{\sqrt{b} - \sqrt{a}}{\sqrt{b} + \sqrt{a}}, \quad \ell = \left(\frac{\sqrt{b} - \sqrt{a}}{\sqrt{b} + \sqrt{a}} \right)^2.$$

It can be verified that $T(I) = -S$ and $T(O) = S$ for S in Theorem 3.3. Then the composition of the Möbius transform and the Zolotarev function $r_k^{(Z)}(T(z))$ achieves the infimum of $Z_k(O, I)$ and is denoted as,

$$(3.6) \quad R_k^{(A)}(z) = R_k^{(Z)}(T(z)) = \left(\frac{1}{z} \right)^k.$$

The infimum of I is taken when $|z| = a$ and the supremum of O is taken when $|z| = b$. Then the infimum of the ratio is $\left(\frac{a}{b}\right)^k$. \square

Theorem 3.5 gives the optimal rational function in solving (2.6). The rational function z^{-k} therein combined with subspace iteration corresponds to the well-known inverse power method. Further, from Theorem 3.5, the radius of \mathcal{D} or the diameter of the annulus is not included in the optimal rational function. Hence, we conclude that, in the sense of convergence rate, the optimal interior eigensolver is the inverse power method if we assume the center of the desired region \mathcal{D} is explicitly known.

While the optimal rational function z^{-k} only has a pole at the origin and could not be written in a sum of low-order rational functions form (2.3). The inverse power method then has to be executed sequentially and could not benefit from the parallelization of distinct poles. In the following, we argue that, although the trapezoidal quadrature of contour integral is not the optimal rational function, it achieves asymptotic optimality in the sense that the ratio \Re of $R_k(z)$ decays at the same rate as that of the optimal rational function up to a constant pre-factor of 2.

We now consider that the contour is the boundary of I and the trapezoidal quadrature with k points is adopted. By Lemma 3.4, the discretization can be written as

$$R_{0,a,k}(z) = \frac{1}{1 + \left(\frac{z}{a}\right)^k},$$

where I is a disk centered at the origin with radius a . By maximum modulus principle, the infimum of I and the supremum of O are taken when $|z| = a$ and $|z| = b$. In region I , $\left|\frac{z}{a}\right|^k \leq 1$. The absolute value of denominator can be viewed as the distance between -1 and $\left(\frac{z}{a}\right)^k$. By simple computation, the infimum is achieved when $z = a$. In a similar way, the supremum of O is achieved when $z = \sqrt[k]{-1}b$ from the fact that $\left|\frac{z}{a}\right|^k > 1$ in O . The ratio (2.5) is

$$\Re = \frac{2}{\left(\frac{b}{a}\right)^k - 1} \sim 2 \left(\frac{a}{b}\right)^k,$$

which asymptotically decays at the same rate as that in [Theorem 3.5](#). The above discussion is summarized in the following corollary.

COROLLARY 3.6. *The trapezoidal quadrature discretization of the contour integral on the boundary of $G = I$ results in the rational function*

$$(3.7) \quad R_k(z) = \frac{1}{1 + \left(\frac{z}{a}\right)^k}.$$

The rational function $R_k(z)$ achieves the ratio $\mathfrak{R} = \frac{2}{\left(\frac{b}{a}\right)^k - 1}$, which is asymptotically equal to the infimum of the min-max problem [\(3.1\)](#) for $E = O$ and $G = I$.

Although the trapezoidal quadrature of the contour integral is not the optimal rational function for [\(3.1\)](#), the ratio asymptotically achieves the optimal one up to a constant prefactor 2. Hence, we call the rational function from the trapezoidal quadrature of the contour the nearly optimal rational function for [\(3.1\)](#). The advantage of the trapezoidal quadrature over the optimal rational function is that [\(3.2\)](#) could be efficiently parallelized in solving the shifted linear systems. Another advantage is as we will propose next that [\(3.2\)](#) admits a composite rule and benefits from the flexible trade-off between the number of matrix factorizations and the iterative linear system solves.

4. Composite rule of trapezoidal quadrature. In this section, we will derive the composite rule of the trapezoidal quadrature discretization of the contour integral and propose eigensolvers based on the composite rule. In the eigensolvers, the composite rule is combined with the multi-shift GMRES to reduce the cost of outer iteration. The proposed eigensolver can reduce cost while preserving the asymptotically optimal ratio \mathfrak{R} .

4.1. Composite rule. Given a positive integer k and its integer factorization $k = k_1 k_2$ for $k_1 > 1$ and $k_2 > 1$, we aim to rewrite the k -th order rational function $R_k(z)$ as a composition of two k_1 -th and k_2 -th rational functions, $R_{k_1}(z)$ and $\hat{R}_{k_2}(z) = R_{k_2}(T(z))$, where $T(\cdot)$ is a simple transform function. Precisely, the composite function admits, $R_{k_1 k_2}(z) = \hat{R}_{k_2}(R_{k_1}(z)) = R_{k_2}(T(R_{k_1}(z)))$.

We restrict $T(\cdot)$ to be a Möbius transform and require it satisfying $T(R_{k_1}(z)) = z^{k_1}$ such that the composition with $R_{k_2}(z)$ becomes obvious. Luckily, we find that the resulting $T(\cdot)$ is easy to be incorporated into the eigensolver design part.

For a Möbius transform function $T(z)$ admits

$$T(z) = \frac{az - b}{cz - d},$$

for a, b, c, d being constant coefficients. According to [Lemma 3.4](#), we have a natural composite expression as,

$$R_{k_1 k_2}(z) = R_1(z^{k_1 k_2}) = R_{k_2}(z^{k_1}).$$

If $T(R_{k_1}(z)) = z^{k_1}$, then directly we have

$$(4.1) \quad R_{k_1 k_2}(z) = R_{k_2}(T(R_{k_1}(z))),$$

which is the desired composite rule.

Now we determine the coefficients such that $T(R_{k_1}(z)) = z^{k_1}$. Substituting $R_{k_1}(z) = \frac{1}{1+z^{k_1}}$ into the expression of $T(z)$, we obtain,

$$\begin{aligned} T(R_{k_1}(z)) &= \frac{a - b(1 + z^{k_1})}{c - d(1 + z^{k_1})} = z^{k_1} \\ \iff dz^{2k_1} + (d - c - b)z^{k_1} + (a - b) &= 0. \end{aligned}$$

The above equality holds for all z . Hence we have solutions of coefficients satisfying $d = 0$ and $a = b = -c$. These solutions of coefficients lead to the unique Möbius transform function,

$$(4.2) \quad T(z) = \frac{1 - z}{z}.$$

The only concern for the above derivation is the case $z = 0$. For rational function $R_k(z)$, zero is achieved $R_k(z) = 0$ if and only if $|z| = \infty$, which is not part of the spectrum of matrices. Hence $z = 0$ for $T(z)$ would not cause any trouble in practice and our composite expression holds for all values of z . In Figure 4.1, the mapping of $R_{k_1}(z)$ and $T(R_{k_1}(z))$ are illustrated.

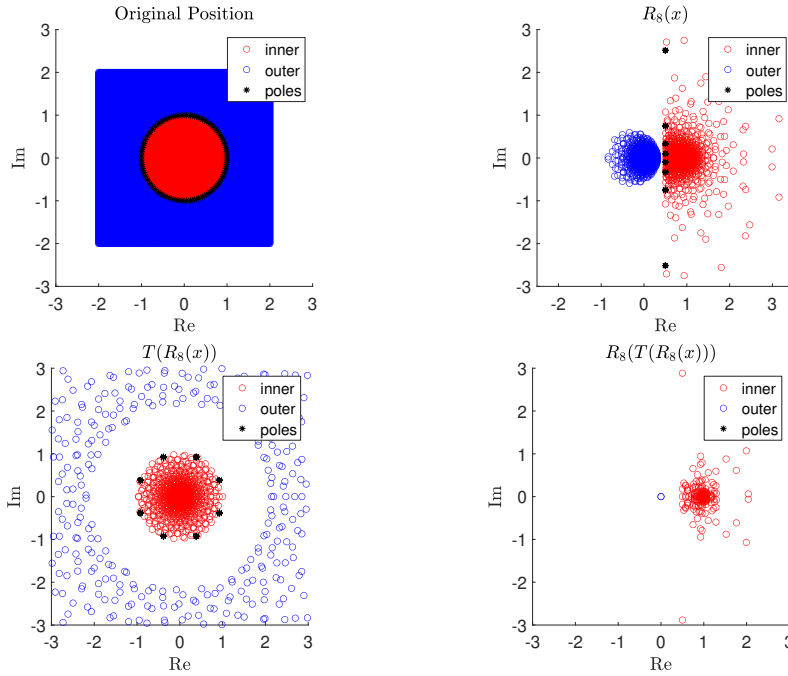


FIG. 4.1. We plot the mapping on $[-2, 2] + [-2, 2] * i$. There are 201 equally spaced points in the direction of real part and imag part, 40401 points in total. The outer points are those $|z| > h = 1.1$ and the inner points are those $|z| \leq 1$ where the contour is $|z| = 1$. We fix the figure window at $[-3, 3] + [-3, 3] * i$ except for top right figure which is shown at $[-2.5, 3.5] + [-3, 3] * i$. Here we let $k_1 = k_2 = 8$ and the poles in all figures are the poles of $R_{k_1 k_2}(z)$. The original eigengap is almost invisible, see top left figure. From top right figure, $R_8(z)$ maps the inner part close to 1 while outer part close to 0 and the poles are mapped on the line $\text{Real}(z) = 0.5$. A more apprent comparison of pre and post-mapping eigengaps is shown as the difference between top left figure and bottom left figure. The composite mapping successfully maps the outer part close to 0 and the inner part close to 1 or modulus greater than 1, see bottom right figure.

Throughout the above derivation, we conclude that $R_{k_1 k_2}(z) = R_{k_2}(T(R_{k_1}(z)))$. A generalized composite rule is given in [Theorem 4.1](#) for domains with various center c and radius r . In [Theorem 4.1](#), we compose $R_{k_2}(\cdot)$ and $T(\cdot)$ together and rewrite it as the sum of first-order rational functions. Such a summation form could later be used directly in the algorithm design.

THEOREM 4.1. *Given a positive integer k and its integer factorization $k = k_1 k_2$, the rational function $R_{c,r,k}(z)$ admits the following composite rule,*

$$R_{c,r,k}(z) = R_{0,1,k_2}(T(R_{c,r,k_1}(z))),$$

where $T(\cdot)$ is the Möbius transform [\(4.2\)](#). When k_2 is even, the rational function $R_{c,r,k}(z)$ further admits the summation form,

$$(4.3) \quad R_{c,r,k}(z) = \sum_{i=1}^{k_2} c_i (R_{c,r,k_1}(z) - s_i)^{-1} R_{c,r,k_1}(z),$$

where $c_i^{(k_2)} = -\frac{1}{k_2} \frac{\sigma_i^{(k_2)}}{1 + \sigma_i^{(k_2)}}$, $s_i^{(k_2)} = \frac{1}{1 + \sigma_i^{(k_2)}}$, and $\{\sigma_i^{(k_2)}\}_{i=1}^{k_2}$ are roots of $x^{k_2} = -1$. When k_2 is odd,

$$(4.4) \quad R_{c,r,k}(z) = \sum_{i=1}^{k_2-1} c_i (R_{c,r,k_1}(z) - s_i)^{-1} R_{c,r,k_1}(z) + \frac{1}{k_2} R_{c,r,k_1}(z),$$

where $\sigma_{k_2}^{(k_2)} = -1$.

[Theorem 4.1](#) could be proved through direct calculation. The detailed proof can be found in [Appendix A](#). Besides the composite rule, there is a connection between the poles of $R_k(z)$ and the poles of the composite rule. The poles of the original rational function are transferred into the poles of the inner operator. The connection is detailed in [Proposition 4.2](#), whose proof is in [Appendix B](#).

PROPOSITION 4.2. *For any $p_i^{(k)}$ being a pole of $R_{c,r,k}(z)$, there exist a $s_j^{(k_2)}$ for $1 \leq j \leq k_2$, such that*

$$(4.5) \quad R_{c,r,k_1}(p_i^{(k)}) = s_j^{(k_2)},$$

where $s_{k_2}^{(k_2)}$ could be infinite when k_2 is odd.

4.2. Interior eigensolver with subspace iteration. Using $R_{c,r,k}(z)$ as the filter in subspace iteration for a matrix pencil (A, B) requires the evaluation of $R_{c,r,k}(B^{-1}A)Y$ for Y being a matrix of size $N \times n_{\text{col}}$. By the composite rule for $R_{c,r,k}(z)$ in [Theorem 4.1](#), the evaluation of $R_{c,r,k}(B^{-1}A)Y$ could be rewritten as,

$$(4.6) \quad R_{c,r,k}(B^{-1}A)Y = \left(\sum_{i=1}^{k_2} c_i (R_{c,r,k_1}(B^{-1}A) - s_i I)^{-1} \right) (R_{c,r,k_1}(B^{-1}A)Y).$$

where the operation $R_{c,r,k_1}(B^{-1}A)Y$ admits,

$$(4.7) \quad R_{c,r,k_1}(B^{-1}A)Y = \sum_{i=1}^{k_1} w_i (p_i B - A)^{-1} B Y$$

for $\{w_i\}$ and $\{p_i\}$ being the weights and poles of $R_{c,r,k_1}(\cdot)$.

In (4.6), there are inner and outer parts of rational function evaluations. For the inner part, as in (4.7), the poles are on the contour and the width of the annulus is determined by the eigengap, which is small in many practical applications. Hence we conclude that linear systems $p_i B - A$ are in general of bad condition numbers. Iterative linear system solvers would often take too many iterations before convergence. Therefore, a direct solver is adopted for all these linear systems. We pre-factorize all linear systems and denote them as $K_i = p_i B - A$ for $i = 1, \dots, k_1$.² Once the factorizations K_i s are available, the inner part could be addressed efficiently. The inner part (4.7) essentially applies a rational filter of the matrix pencil (A, B) and multiplies it to a matrix Y . Without loss of generality, we treat the inner part as a matrix or an operator G acting on Y . Since (4.7) could be evaluated efficiently after the pre-factorization, we know that G could be applied to any Y efficiently.

For the outer part, we first rewrite (4.6) using the operator G ,

$$(4.8) \quad R_{c,r,k}(B^{-1}A)Y = \sum_{i=1}^{k_2} c_i (G - s_i I)^{-1} \tilde{Y}$$

for $\tilde{Y} = G(Y)$. Then it is obvious that (4.8) is in the same form as (4.7) with the matrix pencil replaced by (G, I) . Hence, if we have the explicit matrix representation for G , we could also apply a direct solver to address (4.8). On the other hand, we notice that the condition numbers of linear systems in (4.8) are much smaller than that in (4.7). For linear systems in (4.8), a rational filter with order k_1 has already been applied and the eigengap is enlarged. As shown in Figure 4.1 and also later numerical experiments, the relative eigengap for (G, I) is much enlarged compared to that of (A, B) . Hence, iterative linear system solvers in this case are expected to converge fast. Throughout this paper, we adopt GMRES [14] as the default iterative linear system solver for (4.8) with G been applied as an operator. Recall that GMRES is a Krylov subspace method. By the shift-invariant property of the Krylov subspace, all k_2 shifts in (4.8) could be addressed simultaneously in the same Krylov subspace, i.e.,

$$\begin{aligned} \mathcal{K}_n(G - s_i I, y) &= \mathcal{K}_n(G, y), \\ (G - s_i I)V_n &= V_n(H_{n,n+1} - s_i I_{n,n+1}), \end{aligned}$$

for $i = 1, \dots, k_2$ and V_n denoting the basis of $\mathcal{K}_n(G, y)$. The multi-shift GMRES [1] applies the operator G once per iteration. In all of our numerical experiments, the multi-shift GMRES converges in less than one hundred iterations, and no restarting is needed.

Using a direct solver and an iterative solver for the inner and outer part of (4.6), we obtain an effective algorithm for the rational matrix function filter. Combining this filter with subspace iteration leads to our eigensolver based on the composite rule of the contour integral based rational function, where the contour integral is discretized via the trapezoidal quadrature. Algorithm 4.1 gives the overall pseudocode.

We now estimate the computational cost for Algorithm 4.1. Let C_{factor} and C_{apply} be the computational complexities of the factorization and backward substitution

²Throughout the numerical section of this paper, dense LU factorization is used by default for dense matrices A and B . If A and B are sparse matrices, we adopt the default sparse LU factorization methods in MATLAB.

Algorithm 4.1 Eigensolver: Composite rational function filter

Input: Pencil (A, B) , center c , radius r , number of eigenvalues s , shift σ , number of poles $[k_1, k_2]$.**Output:** the eigenpair (λ_i, x_i) with $\lambda_i \in \mathcal{D}$.

- 1: Compute $\{p_i, w_i\}_{i=1}^{k_1}, \{c_j, s_j\}_{j=1}^{k_2}$.
- 2: **for** $i = 1, \dots, k_1$ **do**
- 3: Pre-factorize $p_i B - A$ as K_i .
- 4: **end for**
- 5: Construct a function for the operation

$$G(Y) = \sum_{i=1}^{k_1} w_i K_i^{-1} B Y.$$

- 6: Generate an orthonormal random matrix $Y^{N \times n_{\text{col}}}$ with $n_{\text{col}} \geq s$.
 - 7: **while** not converge **do**
 - 8: $\tilde{Y} = G(Y)$.
 - 9: Solving $U_j = (G - s_j I)^{-1} \tilde{Y}$ for $j = 1, \dots, k_2$ via multi-shift GMRES.
 - 10: $U = \sum_{j=1}^{k_2} c_j U_j$.
 - 11: $V = \text{orth}(U)$.
 - 12: $W = \text{orth}(AV - \sigma BV)$.
 - 13: $[H_A, H_B, P_L, P_R, V_L, V_R] = \text{qz}(W^* AV, W^* BV)$.
 - 14: $\tilde{\lambda}_i = (H_A)_{i,i} / (H_B)_{i,i}$.
 - 15: $Y = V P_R V_R$.
 - 16: **end while**
-

(solving) of an $N \times N$ matrix. For almost all dense and sparse linear system solvers, the solving complexity is the same as its memory cost. Hence, C_{apply} is also used as the memory cost in storing a factorization.

In the preparation phase before subspace iteration, the weights and poles are computed independent of the matrix, whose computational cost is then $O(1)$. For the pre-factorization of k_1 linear systems, the computation complexity is $k_1 C_{\text{factor}}$ and the memory required is $k_1 C_{\text{apply}}$.

In the subspace iteration phase, the per-iteration computational cost is dominated by the multi-shift GMRES. In the multi-shift GMRES, there are two parts of major computational costs, the construction of orthonormal bases for the Krylov subspace and solving the reduced problems. Since the iteration number for GMRES is bounded by a small constant, the cost in solving the reduced problems is of lower order compared to that of the basis construction part. Hence, we only count the cost for the basis construction part for the multi-shift GMRES. If we denote $n_{\text{iter}}^{(j,t)}$ as the GMRES iteration number for j -th column in the t -th subspace iteration, the dominant computational cost in the GMRES is

$$\sum_{t=1}^T \sum_{j=1}^{n_{\text{col}}} n_{\text{iter}}^{(j,t)} \cdot k_1 C_{\text{apply}},$$

where T is the subspace iteration number, $k_1 C_{\text{apply}}$ is the cost in applying $G(\cdot)$ to a

vector. The leading memory cost is

$$\max_{t=1}^T \sum_{j=1}^{n_{\text{col}}} n_{\text{iter}}^{(j,t)} \cdot N.$$

TABLE 4.1

Computational and memory complexities of the subspace iteration with the simple rational filter and the composite rational filter. The simple rational filter is of order $k_1 k_2$ and the composite rational filter is of inner and outer order k_1 and k_2 respectively. Here C_{factor} and C_{apply} are factorization and solving cost for a matrix of size $N \times N$.

Algorithm	Computation		Memory	
	Pre-Fact	Iteration	Pre-Fact	Iteration
Simple	$k_1 k_2 C_{\text{factor}}$	$T n_{\text{col}} k_1 k_2 C_{\text{apply}}$	$k_1 k_2 C_{\text{apply}}$	$n_{\text{col}} N$
Algorithm 4.1	$k_1 C_{\text{factor}}$	$\sum_{t=1}^T \sum_{j=1}^{n_{\text{col}}} n_{\text{iter}}^{(j,t)} k_1 C_{\text{apply}}$	$k_1 C_{\text{apply}}$	$\max_{t=1}^T \sum_{j=1}^{n_{\text{col}}} n_{\text{iter}}^{(j,t)} N$
Ratio	k_2	$\frac{T n_{\text{col}} k_2}{\sum_{t=1}^T \sum_{j=1}^{n_{\text{col}}} n_{\text{iter}}^{(j,t)}}$	k_2	$\frac{n_{\text{col}}}{\max_{t=1}^T \sum_{j=1}^{n_{\text{col}}} n_{\text{iter}}^{(j,t)}}$

The overall dominant computational and memory costs for Algorithm 4.1 are summarized in Table 4.1. In the same table, we also list the computational and memory costs for subspace iteration with $k_1 k_2$ -th order rational filter without using the composite rule. Another row of ratio is added to indicate the acceleration from Algorithm 4.1. Clearly, both the computation and memory costs in the pre-factorization phase are reduced by a factor of k_2 . While the comparison for the subspace iteration part is less clear. The ratio depends on the iteration numbers of both the subspace iteration and the multi-shifted GMRES. We emphasize that as the subspace iteration goes, the columns of Y become closer and closer aligned with the eigenvectors. The Krylov spaces will converge faster and faster and so is the GMRES, i.e., $\sum_{j=1}^{n_{\text{col}}} n_{\text{iter}}^{(j,t)}$ will decrease fast as t increase.

4.3. Composite rule eigensolver without subspace iteration. The above comparison assumes that we use the same order trapezoidal quadrature with different implements, where the composite rule substitutes the cost of pre-factorization into the solving phase. We can also fix the number of pre-factorizations which in most cases is limited by the memory. Table 4.2 shows the comparison of approximation ratio and the numbers of applying the filter operator G . The simple rule with subspace iteration achieves the asymptotically optimal ratio only if both k_1 and T are large enough. While in practice the k_1 is often limited due to the expensive memory cost in storing the factorizations. In the worst case, k_1 is limited and not large enough to make the ratio smaller than 1. On the other hand, for the composite rule, k_2 is not limited. Increasing k_2 , the GMRES iteration number n_{iter} would increase as well. Such an increase in the iteration number is due to the new shifts. However, as we will show in section 5, n_{iter} is not sensitive to k_2 and increases mildly. With k_2 large enough, the composite rule will achieve the asymptotically optimal ratio in approximation.

Importantly, $T_c = 1$ is sufficient for the composite rule to achieve the target precision when k_2 is sufficiently large. That is a numerically attractive feature of the composite rule. With this feature, we may discard the subspace iteration and only

TABLE 4.2

Convergence rate of and numbers of applying G in a subspace iteration with the simple rational filter and the composite rational filter. The simple rational filter is of order k_1 whereas the composite rational filter is of inner and outer order k_1 and k_2 respectively. Here T_s and T_c are the numbers of subspace iteration for the simple rule and the composite rule.

Algorithm	Separation ratio (2.5)	Number of applying G
Simple	$\left(\frac{2}{(\frac{b}{a})^{k_1}-1}\right)^{T_s}$	$T_s n_{\text{col}}$
Algorithm 4.1	$\left(\frac{2}{(\frac{b}{a})^{k_1 k_2}-1}\right)^{T_c}$	$\sum_{t=1}^{T_c} \sum_{j=1}^{n_{\text{col}}} n_{\text{iter}}^{(j,t)}$
Algorithm 4.2	$\frac{2}{(\frac{b}{a})^{k_1 k_2}-1}$	$\sum_{j=1}^{n_{\text{col}}} n_{\text{iter}}^{(j)}$

increase k_2 when needed. Furthermore, the shifts $s_j^{(k_2)}$ are parts of the shifts $s_j^{(2k_2)}$ and their weights satisfy $c_j^{(k_2)}/2 = c_j^{(2k_2)}$. Therefore, we propose an algorithm parallel to Algorithm 4.1 to double k_2 sequentially as in Algorithm 4.2.

Algorithm 4.2 Eigensolver: Composite rational function filter without subspace iteration

Input: Pencil (A, B) , center c , radius r number of eigenvalues s , shift σ , number of poles k_1 , the initial k_2 suggested to be equal to k_1 , and $k_2 = 0$.

Output: Eigenpair (λ_i, x_i) with $\lambda_i \in \mathcal{D}$.

- 1: Compute $\{p_i, w_i\}_{i=1}^{k_1}, \{c_j, s_j\}_{j=1}^{k_2}$.
- 2: **for** $i = 1, \dots, k_1$ **do**
- 3: Pre-factorize $p_i B - A$ as K_i .
- 4: **end for**
- 5: Construct a function for the operation

$$G(Y) = \sum_{i=1}^{k_1} w_i K_i^{-1} B Y.$$

- 6: Generate an orthonormal random matrix $Y^{N \times n_{\text{col}}}$ with $n_{\text{col}} \geq s$.
- 7: $\tilde{Y} = G(Y)$, U be a zero matrix of the same size.
- 8: **while** not converge **do**
- 9: Solving $U_j = (G - s_j I)^{-1} \tilde{Y}$ for $j = \hat{k}_2 + 1, \dots, k_2$ via multi-shift GMRES with stored Krylov subspace and update the Krylov subspace.
- 10: $U = U/2 + \sum_{j=\hat{k}_2+1}^{k_2} c_j U_j$.
- 11: $V = \text{orth}(U)$.
- 12: $W = \text{orth}(AV - \sigma BV)$.
- 13: $[H_A, H_B, P_L, P_R, V_L, V_R] = \text{qz}(W^* AV, W^* BV)$.
- 14: $\hat{\lambda}_i = (H_A)_{i,i} / (H_B)_{i,i}$.
- 15: $Y = V P_R V_R$.
- 16: $\hat{k}_2 = k_2; k_2 = 2k_2$.
- 17: Compute $\{c_j, s_j\}_{j=\hat{k}_2+1}^{k_2}$.
- 18: **end while**

The key difference between composite rule eigensolvers with and without subspace iteration is the 9th line in Algorithm 4.2. We do not need to regenerate the Krylov subspace from scratch. Instead, we could reuse the Krylov subspace and fur-

ther expand it if the new shifts require a larger Krylov subspace to converge. When k_2 is doubled, the only cost for shifts in the previous iteration is the recalculation of the weights, which is negligible. Hence if $k_2 = K_2$ is sufficient to achieve the desired accuracy for a given problem, the cost of [Algorithm 4.2](#) starting with $k_2 = 1$ is almost the same as that starting with $k_2 = K_2$ for K_2 being a power of two. Comparing [Algorithm 4.2](#) with the simple rule, T_c is always one. Although [Algorithm 4.2](#) could be combined with subspace iteration as well, numerically we found it not necessary. [Algorithm 4.2](#) turns the convergence cost of the subspace iteration into the convergence cost of the multi-shift GMRES. We find that the idea of reusing Krylov subspace for algorithm design is similar to that in [3], where they use a single Cayley transform for preconditioning. Instead, we use trapezoidal quadrature with k_1 poles for preconditioning.

5. Numerical experiment. In this section, we will demonstrate the efficiency and stability of the algorithm we proposed through three experiments. The first experiment shows the advantage of the trapezoidal quadrature discretized contour integrals over another contour integral discretization, Gauss quadrature. The latter two experiments show the computational benefit of applying [Algorithm 4.1](#) and [Algorithm 4.2](#). We test some medium-to-large-scale matrices for illustration purposes. This paper focuses on the design of an efficient filter rather than proposing a novel projection technique. Hence the projection techniques used in [Algorithm 4.1](#), [Algorithm 4.2](#) and HFEAST remain identical.

Throughout the numerical experiments, the relative error of eigenpair is defined as

$$e(\tilde{\lambda}_i, \tilde{x}_i) = \frac{\|A\tilde{x}_i - B\tilde{x}_i\tilde{\lambda}_i\|_2}{(|c| + r)\|B\tilde{x}\|_2},$$

where c and r is the center and radius of the region \mathcal{D} . For the non-Hermitian interior eigenvalue problem, a phenomenon called ghost eigenvalue often appears. The ghost eigenvalue is the one that appears as a computed eigenvalue but not of the original matrix pencil (A, B) . The ghost eigenvalue would make the subspace iteration difficult to converge. There are a lot of practical strategies to address this issue. One of them as in [19] is setting a tolerance τ_g , which is much larger than the target relative error τ . As the iteration goes, the true eigenvalues will converge to a small relative error, while the ghost eigenvalues will not converge to the same precision. After a few steps, there is a gap in the relative errors between true eigenvalues and ghost eigenvalues. When the relative error of an approximate eigenpair $(\tilde{\lambda}_i, \tilde{x}_i)$ inside \mathcal{D} is smaller than τ_g , we view them as the filtered eigenpairs and denote the number of filtered eigenpairs as p . When p is not changed and all relative errors of the filtered eigenpairs are smaller than τ , we terminate the algorithm.

In our experiments, we set $\tau_g = 10^{-2}$ and $\tau = 10^{-8}$. The direct solver is the `lu` function in MATLAB with four outputs under the default setting, which leads to a sparse LU factorization for sparse input matrices. All programs are implemented and executed with MATLAB R2022b. All of the experiments are performed on a server with Intel(R) Xeon(R) Gold 6226R CPU at 2.90 GHz and 1 TB memory. In performance experiments, we report the single-thread wall time.

5.1. Asymptotically optimal rational filter. First we show the ratio (2.5) for the trapezoidal quadrature, Gauss quadrature and the optimal ratio in [Theorem 3.5](#). The numerical results are illustrated in [Figure 5.1](#). Here, we set $a = 1$ and $b = 1.1$.

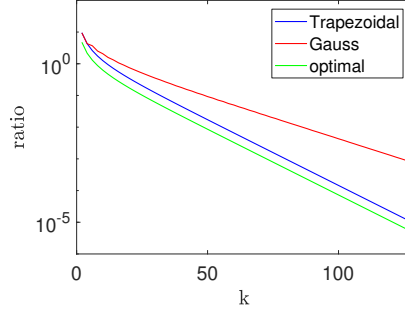


FIG. 5.1. The approximation ratio for various quadrature rules and pole number k s. The pole number k ranges from 2 to 128. Trapezoidal quadrature shows the same slope as optimal ratio, while Gauss quadrature behaves differently.

The infimum of I and supremum of O for Gauss quadrature is not known as a close form, so we use the discretization of 1000 points in both directions of real and imag part on $[-1.5, 1.5] + [-1.5, 1.5] \cdot \imath$ to estimate (2.5) of Gauss quadrature. Only even k is adopted as we perform the Gauss quadrature on the upper semicircle and lower semicircle separately, but not on the full circle directly. Such a Gauss quadrature discretization preserves the symmetry and would perform better than the one that breaks symmetry.

From Figure 5.1, we can find that trapezoidal quadrature always performs better than Gauss quadrature and shows the same decrease order as the optimal ratio comes from the result of Zolotarev. While the Gauss quadrature has a different decrease order from the optimal one.

Now we verify the convergence rate mainly depends on (2.7) via a toy example. On the same region as Figure 5.1, the eigenvalues of test matrices are always keeping four points that the infima of I and suprema of O for trapezoidal and Gauss quadrature is achieved. We had 16 random eigenvalues inside the circle $|z| = 1/b$ and had 80 random eigenvalues on the circle $|z| = b \cdot 1.01$. The eigenvectors matrices are $X = X_1 + \imath X_2$, where X_1 and X_2 are standard Gauss random matrices. We adopt $n_{\text{col}} = 20$, which means the ratio (2.7) is exactly (2.5). We denote $k = 16, 32$ and set the limit of subspace iteration t to be 50. When the number of poles is 16, the ratios of trapezoidal quadrature and Gauss quadrature are 0.5563 and 1.0685, respectively. In this case, the Gauss quadrature fails to capture all the eigenvalues in O while trapezoidal quadrature works. The residual shown is the maximum relative error of filtered eigenpairs, i.e., the approximated eigenpairs whose relative errors are smaller than τ_g .

We remark that the convergence behavior depends on the distribution of eigenvalues. Our analysis in section 3 views the desired spectrum and undesired spectrum as a disk and the complement of a disk. While the eigenvalues of a matrix are discrete points in these regions. It could be the case that the discrete eigenvalues avoid all bad areas in both the numerator and denominator of (2.5) with Gauss quadrature and have a small ratio \mathfrak{R} . In such a case, the rational filter with Gauss quadrature could outperform the rational filter with trapezoidal quadrature for some matrices. While without prior knowledge of the distribution of eigenvalues, the trapezoidal quadrature based filter is a near-optimal choice.

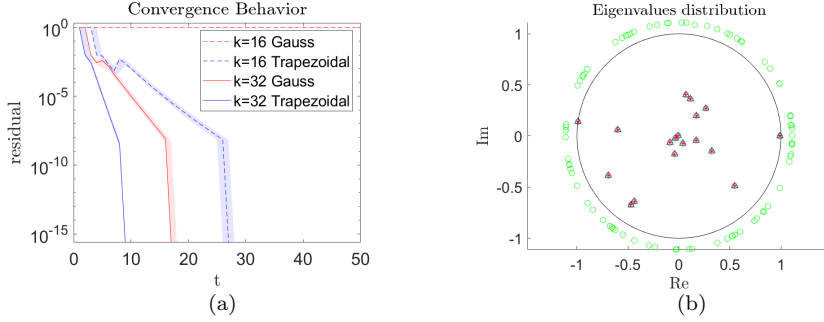


FIG. 5.2. (a) the convergence behavior of trapezoidal quadrature and Gauss quadrature. The points on the line are the median of the residuals at each subspace iteration and the patch parts state the 20-80 quantile of the residuals. (b) one case for Gauss quadrature with 16 poles, it fails to capture all the eigenpairs inside even after 50 subspace iterations. Green points are real eigenvalues. The blue points and red points are the approximated eigenvalues that come from trapezoidal quadrature and Gauss quadrature.

5.2. Composite rule with subspace iteration. The numerical experiment in this section is for [Algorithm 4.1](#), where we set $k_1 = k_2 = 8$ and compare the performance against HFEAST (the subspace iteration with a filter with 64 points). The composite rule can achieve the same accuracy and convergence rate in subspace iteration as that of the simple rule. The composite rule outperforms the simple rule when the cost of factorizations is much more expensive than the cost of solving.

The class of non-Hermitian generalized eigenvalue problems comes from the model order reduction tasks [2, 11] in the circuit simulation [10]. Matrices are constructed based on quasi-two-dimensional square power grids of size $n_x \times n_x \times 10$. The non-Hermitian matrix pencil is (G, C) taking the block form as,

$$G = \begin{bmatrix} G_{11} & G_{12} \\ G_{21} & 0 \end{bmatrix}, \quad C = \begin{bmatrix} C_c & 0 \\ 0 & L \end{bmatrix}.$$

In particular, G_{11} represents the conductance matrix as $G_{11} = L_{n_x} \otimes I_{n_x} \otimes I_{10} + I_{n_x} \otimes L_{n_x} \otimes I_{10} + \frac{1}{10} I_{n_x} \otimes I_{n_x} \otimes L_{10}$, where L_n is a weighted one-dimensional Laplacian matrix of size $n \times n$ as

$$L_n = \frac{n}{100} \begin{bmatrix} 1 & -1 & & & \\ -1 & 2 & -1 & & \\ & \ddots & \ddots & \ddots & \\ & & -1 & 2 & -1 \\ & & & -1 & 1 \end{bmatrix}_{n \times n}$$

and I_n is an identity matrix of size $n \times n$. The off-diagonal blocks of G admit $G_{12} = -G_{21}^\top \in \mathbb{R}^{10n_x^2 \times (20+2n_x^2)}$ with entries being ± 1 or zero. The first 20 columns of G_{12} correspond to 20 input ports at $(\cdot, 1, 1)$ and $(\cdot, n_x, 10)$ two edges, where the corresponding rows have a one. The later $2n_x^2$ columns of G_{12} correspond to inductors. We uniformly randomly pick $2n_x^2$ interior nodes from grid nodes and add an inductor with their neighbor nodes on the same layer. The corresponding G_{12} part is the incidence matrix of the inductor graph. Matrix L is a diagonal matrix of size $20 + 2n_x^2$. The first 20×20 block of L is zero. The later $2n_x^2 \times 2n_x^2$ block has diagonal

entries uniformly randomly sampled from $[0.5, 1.5] \cdot n_x \cdot 10^{-4}$ being the inductance of inductors. The submatrix C_c represents capacitors in the circuit. We add grounded capacitor with 10^{-3} capacitance for each node, which means C_c is a diagonal matrix whose elements are all 10^{-3} . The matrix patterns of G and C are shown in Figure 5.3 for $n_x = 10$.

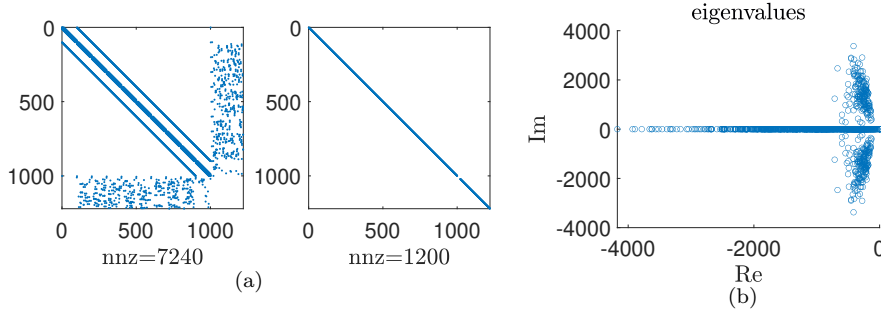


FIG. 5.3. (a) Patterns of G and C when $n_x = 10$; (b) Eigenvalues distribution.

TABLE 5.1

Matrix information. Columns show sizes, number of nonzeros (nnz) of the $G + C$ matrix for various n_x . The centers and radiuses of target regions are included and each encloses 20 eigenvalues. The last column includes the runtime ratio of matrix factorization and solving.

n_x	Size	nnz	(c, r)	ratio
10	1,220	7,440	$(-260 + 1000i, 115)$	33.706
100	120,020	776,040	$(-100 + 23i, 3)$	47.903
200	480,020	3,112,040	$(-14.5 + 27i, 7)$	71.119
400	1,920,020	12,464,040	$(-12 + 26i, 6)$	118.037

Table 5.1 lists detail information about matrices used in our numerical experiments as well as their target regions. The last column of Table 5.1 includes the runtime ratio of the matrix factorization and solving, where the solving runtime is the averaged cost of backward substitutions on a single vector. In all cases, there are 20 eigenvalues in their target regions and we adopt $n_{\text{col}} = 24$. Reference eigenvalues are calculated by `eigs` in MATLAB. The stopping criteria of GMRES is 10^{-9} . Numerical results are reported in Table 5.2. The italic values therein are estimated numbers since the simple rule runs out of memory for those settings. The convergence behaviors are illustrated in Figure 5.4.

The composite rule establishes a trade-off between the number of matrix factorizations and the number of solving in GMRES. When setting $k_2 = 1$, the composite rule falls back to the simple rule. Table 5.2 shows a comparison of the simple rule and the composite rule in two folds: runtime and memory. As shown in the last column of Table 5.1, the runtime ratio between the factorization and the solving grows as the matrix size increases, which is due to the fact that the matrix factorization is of higher complexity compared to that of the solving. Hence, reducing the number of factorizations as in the composite rule would be beneficial. However, as shown in Table 5.2, the simple rule outperforms the composite rule in runtime since the solving dominates the total runtime. When the matrix size further increases, we would see

TABLE 5.2

Runtime (second) of the simple rule and the composite rule for matrices in Table 5.1. Italic values are estimated due to the out-of-memory limit. Comp means the composite rule.

n_x	total		factorization		solving	
	Simple	Comp	Simple	Comp	Simple	Comp
10	1.7×10^0	6.0×10^0	6.2×10^{-1}	7.0×10^{-2}	1.3×10^0	4.8×10^0
100	1.0×10^3	2.6×10^3	4.1×10^2	5.1×10^1	6.2×10^2	2.4×10^3
200	6.8×10^3	1.3×10^4	3.4×10^3	4.2×10^2	3.4×10^3	1.2×10^4
400	<i>4.8×10^4</i>	7.1×10^4	<i>3.0×10^4</i>	3.7×10^3	<i>1.8×10^4</i>	6.4×10^4

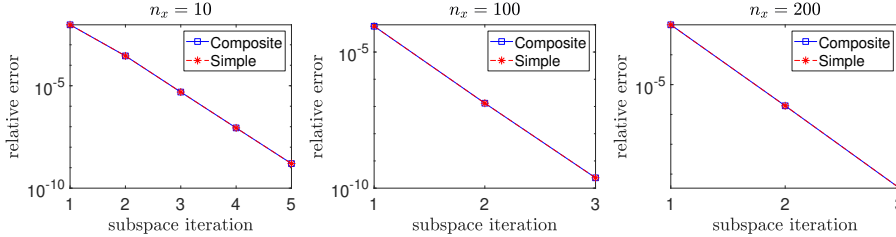


FIG. 5.4. Convergence of the simple rule and the composite rule.

the composite rule outperforms the simple rule in runtime. Regarding the memory cost, the simple rule costs about k_2 times more than that of the composite rule. In this example, we find that the simple rule with $n_x = 400$ already exceeds the memory limit of our computing platform, whereas the composite rule could solve eigenvalue problems with $n_x = 400$ or even larger.

Figure 5.4 shows that the composite rule converges identically as that of the simple rule. This indicates that both the GMRES and the direct solver achieve sufficiently good accuracy. In most cases we have tested, the subspace iteration converges effectively, i.e., usually in a few iterations.

5.3. Composite rule without subspace iteration. This experiment aims to show that with large k_2 , the composite rule will converge without subspace iteration, and the GMRES iteration number does not increase dramatically when k_2 increases. Such an observation means the strategy doubling k_2 each time in Algorithm 4.2 would be affordable compared to the case with optimal k_2 . Throughout this section, we reuse matrix pencils in subsection 5.2. We perform three algorithms in this section: the simple rule with $k = 8$, the composite rule with $k_1 = 8$ and various choices of fixed k_2 (Algorithm 4.1), and Algorithm 4.2 with $k_1 = 8$. Also, various choices of n_{col} are explored.

Table 5.3 reports the runtime of the simple rule and Algorithm 4.2, and Figure 5.5 illustrates the relative runtime of Algorithm 4.1 for various k_2 . The relative runtime of Algorithm 4.2 could be read from Figure 5.5 from those first triangle marks at k_2 being a power of two.

In Table 5.3, all three choices of n_{col} overestimates the actual number of eigenvalues in the region. The simple rule with a fixed $k = 8$ fails to converge when n_{col} is not sufficiently large. In contrast, Algorithm 4.2 converges in all scenarios. Based on this experiment and other experiments we tried but not listed in the current paper, the convergence of the simple rule is sensitive to the choice of two hyperparameters,

TABLE 5.3

Runtime (second) of the simple rule and [Algorithm 4.2](#). Notation “inf” denotes the case where target eigenpairs are not all captured.

n_x	$n_{\text{col}} = 21$		$n_{\text{col}} = 22$		$n_{\text{col}} = 24$	
	Simple	Composite	Simple	Composite	Simple	Composite
100	inf	9.9×10^2	1.3×10^3	1.1×10^3	9.8×10^2	1.1×10^3
200	inf	5.3×10^3	inf	5.5×10^3	6.9×10^3	6.0×10^3
400	7.2×10^4	3.1×10^4	4.4×10^4	3.1×10^4	3.1×10^4	3.4×10^4

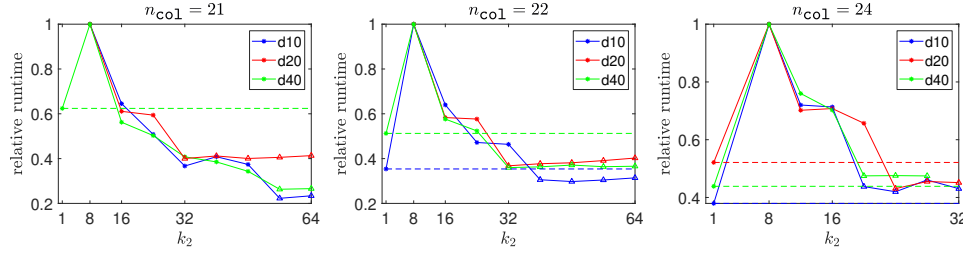


FIG. 5.5. Relative runtime of [Algorithm 4.1](#) with $k_1 = 8$ and various k_2 . The star marks denote those subspace iterations converge in more than one iteration, whereas the triangle marks denote those without subspace iteration. When $k_2 = 1$, [Algorithm 4.1](#) is equivalent to the simple rule.

k and n_{col} . While the convergence of [Algorithm 4.2](#) is not sensitive to the choice of k_1 and n_{col} .³ In the worst-case scenario, when the given region is enclosed by many unwanted eigenvalues, mildly increasing n_{col} would not resolve the convergence issue in the simple rule. However, [Algorithm 4.2](#) can converge robustly. When both the simple rule and [Algorithm 4.2](#) converge, we notice that [Algorithm 4.2](#) outperforms the simple rule for small n_{col} . When n_{col} increases, these two methods become comparable on runtime.

[Figure 5.5](#) explores the optimal choice of k_2 without subspace iteration, i.e., the first triangle marks on each curve. We find that the optimal k_2 is not necessary $2^p k_1$ as in [Algorithm 4.2](#). Besides the factorization cost, the dominating computing cost of the composite rule is the multi-shift GMRES iterations, i.e., the number of applying G (4.6). Increasing k_2 would add more shifts to the multi-shift GMRES but not necessarily increase iteration number, and the extra cost of orthogonalization is negligible compared to that of applying G . In all curves in [Figure 5.5](#), we observe that, after their first triangle marks, the relative runtime mostly stays flat and increases extremely slowly. Hence, even if [Algorithm 4.2](#) is not using the optimal k_2 , the runtime of [Algorithm 4.2](#) is almost the same as that with optimal k_2 . We conclude that [Algorithm 4.2](#) is an efficient and robust eigensolver and is more preferred than [Algorithm 4.1](#).

Remark 5.1. We remark on the hyperparameter choices in [Algorithm 4.2](#). Given a matrix pencil and a region, an overestimation n_{col} of the number of eigenvalues is required. If we perform factorizations and solvings sequentially, we may need to choose a proper k_1 depending on whether factorizations are more expansive than that of solving. In the view of parallel computing, the k_1 factorizations and solvings are

³The requirement for n_{col} is that n_{col} is an overestimation of the number of eigenvalues in the region.

ideally parallelizable. Hence, we would set k_1 as large as possible to fully use the computation resource and reduce the GMRES iterations.

6. Conclusion. This paper finds the optimal separation rational function via the Zolotarev function. The optimal rational function leads to the traditional inverse power method in numerical linear algebra. Discretizing the contour integral with the standard trapezoidal quadrature results in an asymptotically optimal separation rational function. The numerical algorithm based on the trapezoidal quadrature (the simple rule) admits natural parallel computing property, while the inverse power method is sequential. Hence, the simple rule would benefit more from modern multi-core computer architecture. Further, we show the composite rule of the trapezoidal quadrature, i.e., $R_{k_1 k_2}(z) = R_{k_2}(T(R_{k_1}(z)))$ for $R_k(\cdot)$ being the simple rule of order k and $T(\cdot)$ being a simple Möbius transform.

Based on the composite rule, we propose two eigensolvers for the generalized non-Hermitian eigenvalue problems, [Algorithm 4.1](#) and [Algorithm 4.2](#). Both algorithms adopt direct matrix factorization for the inner rational function evaluation and multi-shift GMRES for the outer rational function. Compared to the simple rule with the same number of poles, both composite-rule-based algorithms reduce the number of factorizations and reduce the memory requirement in solving eigenvalue problems. This is of fundamental importance when matrices are of large scale. The difference between the two composite algorithms is the subspace iteration. In [Algorithm 4.1](#), both k_1 and k_2 are hyperparameters, and the algorithm adopts the subspace iteration to converge to desired eigenpairs. In contrast, [Algorithm 4.2](#) is designed without subspace iteration. [Algorithm 4.2](#) adopts k_1 as a hyperparameter and gradually increases k_2 until the rational function approximation is accurate enough and the algorithm converges to desired eigenpairs without subspace iteration. As k_2 increases in [Algorithm 4.2](#), by the property of multi-shift GMRES, the number of GMRES iterations, i.e., the number of applying G , increases very mildly. Hence, compared to the simple rule and [Algorithm 4.1](#), [Algorithm 4.2](#) is a robust and efficient eigensolver.

We demonstrate the efficiency of proposed algorithms via both small-scale and large-scale, synthetic and practical generalized non-Hermitian eigenvalue problems. Numerical results show that [Algorithm 4.1](#) outperforms the simple rule only if the matrix factorization is much more expensive than the solving. The convergence of [Algorithm 4.2](#) is not sensitive to hyperparameter n_{col} and k_1 . In terms of the runtime, [Algorithm 4.2](#) either outperforms or is comparable to the simple rule. A suggestion for the hyperparameter choices of [Algorithm 4.2](#) is also provided based on both the analysis and numerical results.

Acknowledgement. This work is supported in part by the National Natural Science Foundation of China (12271109) and Shanghai Pilot Program for Basic Research - Fudan University 21TQ1400100 (22TQ017).

Appendix A. Proof of [Theorem 4.1](#).

Proof. We can use the equation $z = ry + c$ to transfer the contour discretization on an arbitrary circle into the case of the unit circle around origin. The rational function then admits,

$$(A.1) \quad R_{c,r,k}(z) = R_{0,1,k}(y).$$

Combining with the composite rule [\(4.1\)](#), we have

$$(A.2) \quad R_{c,r,k}(z) = R_{0,1,k_1 k_2}(y) = R_{0,1,k_2}(T(R_{0,1,k_1}(y))) = R_{0,1,k_2}(T(R_{c,r,k_1}(z))).$$

TABLE C.1

Number of solvings and GMRES iteration in the simple rule and the composite rule. *Italic values are estimated due to the out of memory limit.*

n_x	Simple	Composite	
	Solving	n_{iter}	Solving
10	[1536,1536,1536,1536,1536]	[38,32,30,30,30]	[7296,5824,5208,4888,4160]
100	[1536,1536,1536]	[39,33,32]	[7488,5600,4816]
200	[1536,1536,1536]	[38,31,29]	[7232,5264,4288]
400	[1536, 1536, 1536]	[37,32,31]	[7064,5432,3816]

Now we turn to prove the summation form. We use the convention $R_k(z) = R_{0,1,k}(z)$ that corresponds to the illustration in the body. When k_2 is even, there is $\sigma_i^{(k_2)} \neq -1$. With [Lemma 3.4](#), the summation form is,

$$\begin{aligned}
 R_{c,r,k_1 k_2}(z) &= R_{k_2}(T(R_{c,r,k_1}(y))) = \frac{1}{k_2} \sum_{i=1}^{k_2} \frac{\sigma_i^{(k_2)}}{\sigma_i^{(k_2)} - \frac{1-R_{c,r,k_1}(y)}{R_{c,r,k_1}(y)}} \\
 &= \frac{1}{k_2} \sum_{i=1}^{k_2} \frac{\sigma_i^{(k_2)} R_{c,r,k_1}(y)}{(1 + \sigma_i^{(k_2)}) R_{c,r,k_1}(y) - 1} \\
 &= \frac{1}{k_2} \sum_{i=1}^{k_2} \frac{\sigma_i^{(k_2)}}{1 + \sigma_i^{(k_2)}} (R_{c,r,k_1}(z) - \frac{1}{1 + \sigma_i^{(k_2)}})^{-1} R_{c,r,k_1}(x) \\
 &= \sum_{i=1}^{k_2} c_i (s_i^{(k_2)} - R_{c,r,k_1}(z))^{-1} R_{c,r,k_1}(z),
 \end{aligned}
 \tag{A.3}$$

where

$$c_i^{(k_2)} = -\frac{1}{k_2} \frac{\sigma_i^{(k_2)}}{1 + \sigma_i^{(k_2)}}, \quad s_i^{(k_2)} = \frac{1}{1 + \sigma_i^{(k_2)}}.
 \tag{A.4}$$

When k_2 is odd, the term associated with $\sigma_{k_2}^{(k_2)} = -1$ in summation form is equal to $\frac{1}{k_1} R_{k_1}$. \square

Appendix B. Proof of [Proposition 4.2](#).

Proof. By [Lemma 3.4](#), we know

$$R_{c,r,k_1}(p_i^{(k)}) = R_{0,1,k_1}(\sigma_i^{(k)}) = \frac{1}{1 + (\sigma_i^{(k)})^{k_1}} = \frac{1}{1 + \sigma_j^{(k_2)}} = s_j^{(k_2)}. \quad \square
 \tag{B.1}$$

Appendix C. GMRES iteration number. As we mentioned in [subsection 4.2](#), the multi-shift GMRES will converge faster as the subspace iteration converges. [Table C.1](#) reports the number of solving in both the simple and the composite rules and its GMRES iteration number. The normalized last column of [Table C.1](#) is visualized in [Figure C.1](#).

[Table C.1](#) shows that the number of solving in each subspace iteration in the simple rule stays constant, whereas that for the composite rule decreases. Notice that

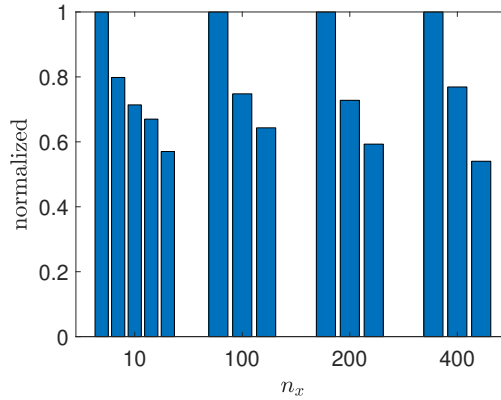


FIG. C.1. Normalized solving cost in the composite rule.

the n_{iter} decays much slower than the number of solving in the composite rule. We have two remark points. The first point is that different shifts converge in different numbers of iterations, and n_{iter} is the maximum number of GMRES iterations among all shifts. The second point is that different columns converge to eigenvectors with different rates, and the n_{iter} shown here is the maximum number of iterations among all columns. The difference in the decays is mainly due to the second point.

REFERENCES

- [1] T. BAKHOS, P. K. KITANIDIS, S. LADENHEIM, A. K. SAIBABA, AND D. B. SZYLD, *Multipreconditioned gmres for shifted systems*, SIAM Journal on Scientific Computing, 39 (2017), pp. S222–S247, <https://doi.org/10.1137/16M1068694>.
- [2] P. GROSS, R. ARUNACHALAM, K. RAJAGOPAL, AND L. PILEGGI, *Determination of worst-case aggressor alignment for delay calculation*, in 1998 IEEE/ACM International Conference on Computer-Aided Design. Digest of Technical Papers (IEEE Cat. No.98CB36287), 1998, pp. 212–219, <https://doi.org/10.1145/288548.288616>.
- [3] R. HUANG, J. SUN, J. SUN, AND C. YANG, *Recursive integral method with cayley transformation*, Numerical Linear Algebra with Applications, 25 (2017).
- [4] T. IKEGAMI AND T. SAKURAI, *CONTOUR INTEGRAL EIGENSOLVER FOR NON-HERMITIAN SYSTEMS: A RAYLEIGH-RITZ-TYPE APPROACH*, Taiwanese Journal of Mathematics, 14 (2010), pp. 825 – 837, <https://doi.org/10.11650/twjm/1500405869>.
- [5] T. IKEGAMI, T. SAKURAI, AND U. NAGASHIMA, *A filter diagonalization for generalized eigenvalue problems based on the sakurai-sugiura projection method*, Journal of Computational and Applied Mathematics, 233 (2010), pp. 1927–1936, <https://doi.org/10.1016/j.cam.2009.09.029>.
- [6] J. KESTYN, E. POLIZZI, AND P. T. PETER TANG, *Feast eigensolver for non-hermitian problems*, SIAM Journal on Scientific Computing, 38 (2016), pp. S772–S799, <https://doi.org/10.1137/15M1026572>.
- [7] R. B. LEHOUCQ, D. C. SORENSEN, AND C. YANG, *Arpack users' guide - solution of large-scale eigenvalue problems with implicitly restarted arnoldi methods*, in Software, environments, tools, 1998.
- [8] Y. LI AND H. YANG, *Interior eigensolver for sparse hermitian definite matrices based on zolotarev's functions*, Communications in Mathematical Sciences, 19 (2021), pp. 1113–1135.
- [9] C. B. MOLER AND G. W. STEWART, *An algorithm for generalized matrix eigenvalue problems*, SIAM Journal on Numerical Analysis, 10 (1973), pp. 241–256, <https://doi.org/10.1137/0710024>.
- [10] F. N. NAJM, *Circuit Simulation*, Wiley-IEEE Press, 2010.
- [11] ODABASIOGLU, CELIK, AND PILEGGI, *Prima: passive reduced-order interconnect macromodeling algorithm*, in 1997 Proceedings of IEEE International Conference on Computer Aided

- Design (ICCAD), 1997, pp. 58–65, <https://doi.org/10.1109/ICCAD.1997.643366>.
- [12] P. P. PETRUSHEV AND V. A. POPOV, *Rational Approximation of Real Functions*, Encyclopedia of Mathematics and its Applications, Cambridge University Press, 1988, <https://doi.org/10.1017/CBO9781107340756>.
 - [13] E. POLIZZI, *Density-matrix-based algorithm for solving eigenvalue problems*, Phys. Rev. B, 79 (2009), p. 115112, <https://doi.org/10.1103/PhysRevB.79.115112>.
 - [14] Y. SAAD, *Iterative Methods for Sparse Linear Systems*, Society for Industrial and Applied Mathematics, second ed., 2003, <https://doi.org/10.1137/1.9780898718003>.
 - [15] T. SAKURAI AND H. SUGIURA, *A projection method for generalized eigenvalue problems using numerical integration*, Journal of Computational and Applied Mathematics, 159 (2003), pp. 119–128, [https://doi.org/10.1016/S0377-0427\(03\)00565-X](https://doi.org/10.1016/S0377-0427(03)00565-X).
 - [16] G. STARKE, *Near-circularity for the rational zolotarev problem in the complex plane*, Journal of Approximation Theory, 70 (1992), pp. 115–130, [https://doi.org/10.1016/0021-9045\(92\)90059-W](https://doi.org/10.1016/0021-9045(92)90059-W).
 - [17] G. W. STEWART, *A krylov-schur algorithm for large eigenproblems*, SIAM Journal on Matrix Analysis and Applications, 23 (2002), pp. 601–614, <https://doi.org/10.1137/S0895479800371529>.
 - [18] G. YIN, *A harmonic feast algorithm for non-hermitian generalized eigenvalue problems*, Linear Algebra and its Applications, 578 (2019), pp. 75–94, <https://doi.org/10.1016/j.laa.2019.04.036>.
 - [19] G. YIN, R. H. CHAN, AND M.-C. YEUNG, *A feast algorithm with oblique projection for generalized eigenvalue problems*, Numerical Linear Algebra with Applications, 24 (2017), p. e2092, <https://doi.org/10.1002/nla.2092>.